International Journal of Biological Macromolecules 233 (2023) 123567

Contents lists available at ScienceDirect

International Journal of Biological Macromolecules

journal homepage: www.elsevier.com/locate/ijbiomac

Cellulose nanofiber-based multifunctional films integrated with carbon dots and anthocyanins from *Brassica oleracea* for active and intelligent food packaging applications

Rajesh V. Wagh [a,b], Ajahar Khan [b], Ruchir Priyadarshi [b], Parya Ezati [b], Jong-Whan Rhim [b,*]

[a] *Department of Livestock Products Technology, College of Veterinary Science, Guru Angad Dev Veterinary and Animal Sciences University, Ludhiana, Punjab 14004, India*

[b] *BioNanocomposite Research Center, Department of Food and Nutrition, Kyung Hee University, Seoul 02447, Republic of Korea*

ARTICLE INFO

Keywords:
Carbohydrate polymer
Cellulose nanofiber
Anthocyanin
Carbon dots
Nanocomposite
Intelligent packaging

ABSTRACT

A new generation of carbon dot-based active and intelligent packaging films with UV blocking, antibacterial, and real-time sensing potentials was fabricated using *Brassica oleracea* (BO) extract. The cellulose nanofiber (CNF) was used to prepare the multifunctional intelligent nanocomposite film integrated with BO anthocyanins (BOA) and BO-biowaste-derived carbon dots (BO-CDs). The incorporation of 1.5 % BO-CD and 6 % BOA in the CNF matrix improved the physicochemical and UV blocking (>189 % increase) properties of the fabricated films. The synthesized BO-CD exhibits high fluorescence, UV absorption, antibacterial and antioxidant functions. It showed strong radical scavenging activity against ABTS (~90 %) and DPPH (~80 %) compared to the neat CNF film. Scanning electron microscopy and X-ray photoelectron spectroscopy (XPS) have shown enhanced compatibility and elemental composition of the BO-CDs/BOA additives in the CNF-polymer matrix. Packaging tests showed that the prepared film worked efficiently and non-destructively and was able to monitor the freshness of minced pork, fish, and shrimp in real-time through a distinct visual change from red to colorless/yellow during storage at 25 °C for 48 h. Active and intelligent films developed based on CNF/BO-CDs/BOA are expected to be applied as multifunctional packaging materials that can indicate quality changes and extend the shelf life of packaged perishable foods.

1. Introduction

Preserving food quality and reducing waste in the supply chain is a challenge for the global food industry. Consumer demand for fresh, hygienic, high-quality food and real-time quality monitoring is becoming popular [1]. Smart packaging, which replaces the status quo of traditional food packaging, can be divided into intelligent packaging and active packaging [2–4]. Active packaging preserves or enhances food quality while extending its shelf life, while intelligent packaging monitors the freshness of the packaged food [5]. The intelligent indicators, such as TT (temperature & time) indicators [6] and gas indicators [7] or pH indicators [4,8,9], can be embedded in packaging polymers or mounted to the inside of a container. Above all, halochromic pH indicators provide advantages, including economy, portability, safety, and sensitivity [10,11]. Anthocyanins are used as a natural pH-dependent color change indicator of food freshness [4,7–9].

Brassica oleracea comes under the Brassicaceae family and is cultivated in many parts of the world [12]. It is a source of anthocyanins, containing cyanidin, petunidin, delphinidin, pelargonidin, and peonidin, which exhibit characteristic halochromic changes under different pH [12,13]. This broad color response, therefore, makes it a promising natural pH/halochromic indicator candidate, especially for intelligent food packaging [1,13,14]. The recent studies on anthocyanin-based intelligent films are summarized in Table S1.

Plant anthocyanins are widely used in smart food packaging [12,15]. Recovery and extraction of anthocyanins are critical and influenced by input variables such as solvent, extraction time, temperature, *etc.*, along with the desired output responses [16]. The quickest and most effective one-step method for optimizing the effect of extraction conditions while considering the interaction effect on the desired response is the Response Surface Methodology (RSM). RSM has been frequently used to improve the operational protocols of various plant materials to obtain

* Corresponding author.
E-mail address: jwrhim@khu.ac.kr (J.-W. Rhim).

https://doi.org/10.1016/j.ijbiomac.2023.123567
Received 1 December 2022; Received in revised form 2 February 2023; Accepted 2 February 2023
Available online 7 February 2023

potent anthocyanin-rich extracts [16]. Therefore, state-of-the-art technology has been established to develop green extraction procedures assisted by RSM to achieve faster extraction with higher anthocyanin yields.

According to the UN-Food Waste Index Report 2021–22, fruits and vegetables account for nearly 50 % of household food waste [17]. Converting food waste into novel nanomaterials such as green carbon dots (CDs) for various applications is a promising approach for '*waste to wealth*' [18–20]. Using green synthesis methods, scientists have effectively synthesized CDs from biowaste resources such as orange peels [21] and watermelon peels [22]. CD's role as an innovative active ingredient in smart packaging films has been widely documented as a UV blocker [23], antimicrobial agent [18,24], and antioxidant [21]. The ability of these smart packages to enhance the mechanical attributes of films and prevent microbial contamination/proliferation guarantees food protection [18]. At the same time, it preserves the biopolymer itself from microbial degradation [21].

The current study aimed to fabricate an intelligent halochromic biodegradable indicator film using environmentally friendly, RSM-optimized *Brassica oleracea* anthocyanin (BOA). In addition, bio-waste (BO-leftover after anthocyanin extraction) derived BO-CDs were used to functionalize the cellulose nanofibers (CNF) polymers to develop halochromic indicator films. Finally, the developed multifunctional halochromic indicator films were employed for quality monitoring using *in vivo* food models of fish, minced pork, and shrimp at 25 °C.

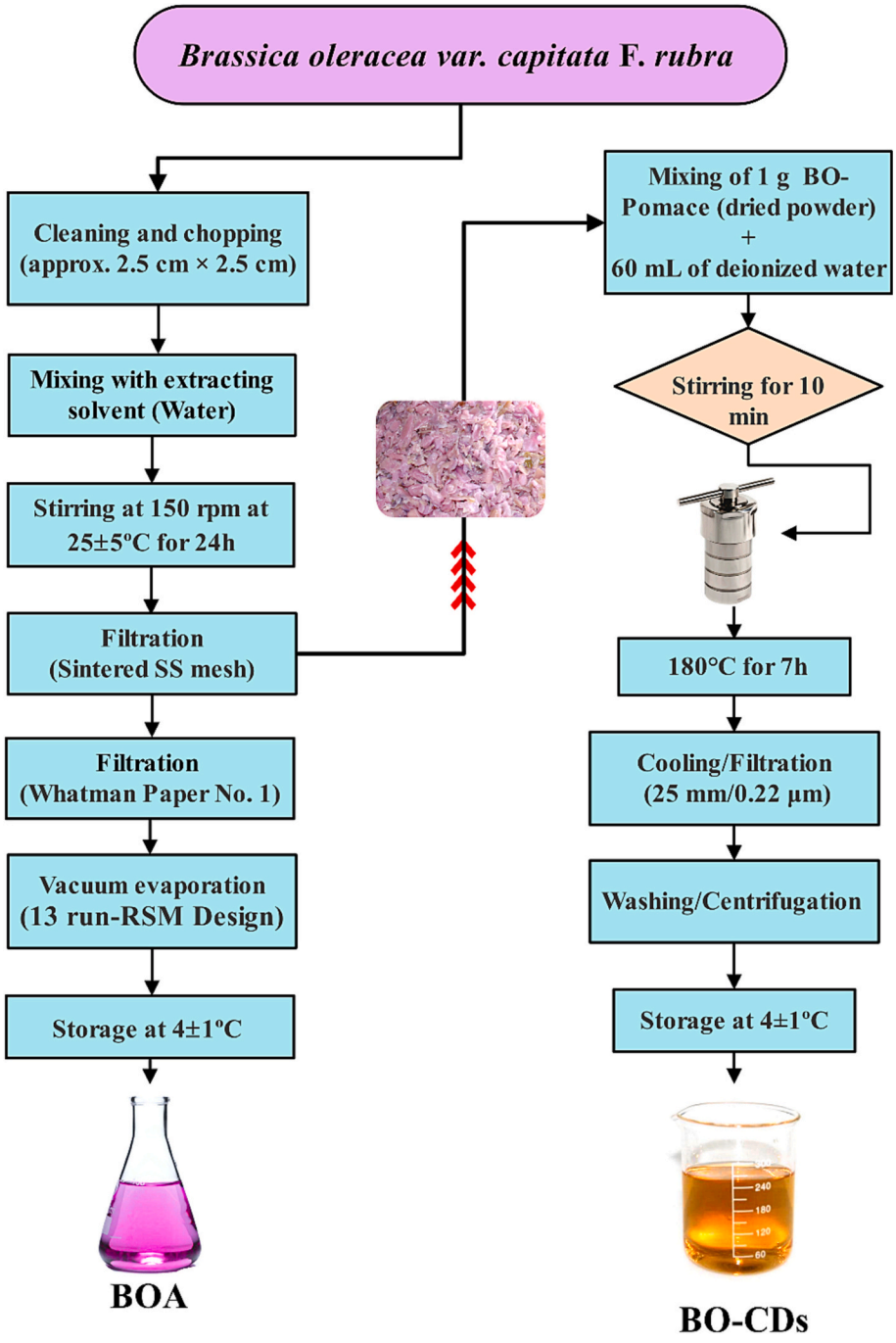

Scheme 1. Process for preparing anthocyanin (BOA) and carbon dots (BO-CDs).

2. Materials and methods

2.1. Materials

Fresh *Brassica oleracea* (red cabbage) was procured from a local market (Seoul, Republic of Korea). Cellulose nanofiber (TEMPO-CNF, width: 10–20 nm, length: 3–350 μm, viscosity (0.75 wt%): 2000 cPs) was obtained from Moorim Co. Ltd. (Ulsan, Republic of Korea). Pure culture of *L. monocytogenes* ATCC 15313 and *E. coli* O157: H7 ATCC 43895, procured from the Korean Collection for Type Culture (KCTC, Seoul, Korea). Ethanol (98 %), acetone (98 %), 2,2′-azino-bis-(3-ethylbenzothiazoline-6-sulfonic acid) ($ABTS^{\bullet+}$), 2,2-diphenyl-1-picrylhydrazyl ($DPPH^{\bullet}$), and potassium persulfate were procured from Sigma-Aldrich (St. Louis, MO, USA). All the analytical chemicals were procured from Sigma- Aldrich and Daejung chemicals and metals Co., Ltd. (Siheung, Gyeonggi-do, Republic of Korea).

2.2. Preparation of anthocyanin extract and BO-CDs

The response surface-optimized extraction of anthocyanin was carried out according to the method described by [22] with slight modifications. In detail, as shown in Scheme 1, fresh *Brassica oleracea* was cleaned and cut into 2.5 × 2.5 cm sizes. The bio-waste residue of *Brassica oleracea* after anthocyanin extraction was further used to synthesize BO-CDs through one step hydrothermal approach [19], as shown in Scheme 1.

2.3. Fabrication of CNF and CNF/BO-CDs/BOA indicator films

The film-forming solution was prepared by dissolving 4 g of CNF in 145 mL distilled water and 30 % (w/w) glycerol and stirred vigorously at 70 °C for 25 min. The solution was cooled down to 45 °C and added with 6.0 % (w/w) of BOA followed by 1.5 % (w/w) of BO-CDs and stirred for 35 min. The solution was cast on a Teflon-glass plate (24 cm × 30 cm), dried at room temperature (23 ± 2 °C) for 48 h, and dried films were peeled off and stored at 25 °C/50 % RH till further use. The fabricated films were designated as the neat CNF (control films without BOA/BO-CDs and CNF/BO-CDs/BOA. Methods for characterization and property measurement of film samples are provided in the Supporting information.

2.4. Statistical analysis

Each treatment film was prepared in triplicate, each parameter was evaluated in duplicate, and the results were presented as mean ± SD (standard deviation). The experimental data were analyzed statistically using Design Expert software (Stat-Ease, Inc., Minneapolis, USA) and SPSS-24 (IBM-SPSS Statistics, NY, USA) software packages. The significant differences among the film properties were determined at a 95 % confidence level ($p < 0.05$) with Duncan's multiple range test.

3. Results and discussion

3.1. Response surface optimization of extraction protocols for BOA

The comparative efficacy of BOA in terms of Total anthocyanin contents (monomeric), $ABTS^{\bullet+}$ and $DPPH^{\bullet}$ scavenging activity with different solvents, *viz.* water, 80 % ethanol, and 80 % acetone, varied significantly ($p < 0.05$) with the types of solvent used. Results indicated that among the three solvents used, water extract exhibited the highest antioxidant activities, followed by ethanol and acetone. Based on these preliminary tests, we selected water as the extraction solvent for further experiments and formulated the coded/noncoded factors (Table S2). Central Composite Design (CCD) suggested 13 experimental (Table S3) runs with varying processing protocols as vacuum evaporator extracting time and temperature against the responses, *i.e.*, Total anthocyanin content (monomeric) TAC (mg Cy3G/100 g FW), $ABTS^{\bullet+}$ (%) and $DPPH^{\bullet}$ (%). The resulting data were fitted, and analysis of variance (ANOVA) was plotted along with 3D surface plots.

3.1.1. Model fitting

Obtained data were fitted into the second-order polynomial equations by evaluating each independent variable as a function of quadratic, linear, and interaction response. The ANOVA concluded with high *F*-values (>0.8) and low *p*-values (<0.0001) for the studied responses (Table 1). The CV values (0.56–1.04) for the proposed models indicated the high precision and reliability of the experiments. In addition, high R^2 values (>0.90) and non-significant 'Lack of Fit' ($p > 0.05$) indicated that the quadratic model was highly significant to obtained data and capable of describing the relationship (desirability > 0.955) between the extraction conditions and responses [16].

3.1.2. TAC, ABTS •+ and DPPH• scavenging activity

The response surface analysis demonstrated that the studied factors had a quadratic relationship with a good regression coefficient between TAC, $ABTS^{\bullet+}$, and $DPPH^{\bullet}$ scavenging activity. The obtained model showed the relationship as shown below for TAC (Eq. (1)), $ABTS^{\bullet+}$ (Eq. (2)), and $DPPH^{\bullet}$ scavenging activity (Eq. (3)):

$$TAC = 104.54 + 0.71A - 0.91B - 1.21AB - 2.73A^2 - 3.68B^2 \quad (1)$$

$$ABTS^{\dot{+}} = 47.94 + 0.84A - 0.78B - 1.01AB - 2.44A^2 - 3.39B^2 \quad (2)$$

$$DPPH\doteq 42.00 + 0.81A - 0.91B - 1.05AB - 2.33A^2 - 3.60B^2 \quad (3)$$

The analysis of variance showed that the extracting time and extracting temperature had significant linear, quadratic, and interaction effects ($p < 0.0001$) on TAC, $ABTS^{\bullet+}$, and $DPPH^{\bullet}$ scavenging activities. The model (Table 1) suggested that varying extracting time (10-20 min) and temperature (60–120 °C) significantly affected the extraction of total anthocyanins and phenolic compounds from *Brassica oleracea*, which would effectively scavenge free radicals [23]. The 3D surface plots showed the effect of extracting time and temperature on the $ABTS^{\bullet+}$ (Fig. 1a), $DPPH^{\bullet}$ scavenging (Fig. 1b), and TAC (Fig. 1c) contents, which increased linearly with the increased extracting time (16 min) and temperature up to a fixed flag spot (85 °C), followed by a declined trend with a further increase in time and temperature.

This behavior concerning increasing temperature and time can be hypothesized using the three mechanisms [24]. First, due to moderate heating, insoluble phenolic molecules (cyanidin) may be liberated (deglycosylation) when the lignin bonds to phenolic acids are disrupted [25]. Secondly, insoluble phenolic and lignin may be degraded at high temperatures due to increased mass solubility and diffusion coefficient, giving rise to more phenol derivatives (phloroglucinaldehyde and hydroxybenzoic acid) [23]. Lastly, at high temperatures with prolonged time, thermal degradation of the polyphenols may occur [26]. Thermal degradation is the most common mechanism to explain the cleavage in polyphenolic rings during high-temperature extractions [27], as shown in Fig. 1d. Nevertheless, an upper-temperature limit must be considered to prevent the decomposition of thermo-sensitive compounds [16]. Ideal extraction temperatures between 80 and 90 °C have been reported by other researchers, which are consistent with the temperatures investigated in our experiments [12,27].

The response surface analyses depicted that maximum TAC, $ABTS^{\bullet+}$, and $DPPH^{\bullet}$ scavenging activity can be obtained at a defined extraction time of 16.0 min and extraction temperature of 85.45 °C, leading to 104.66 mg Cy3G/100 g FW of TAC, 48.08 % of $ABTS^{\bullet+}$ and 42.15 % of $DPPH^{\bullet}$ activity. By employing the optimized extraction protocols, we prepared a potent *Brassica oleracea* anthocyanins-rich extract, which was further used to develop a halochromic indicator.

Table 1
ANOVA and regression coefficients of the second-order polynomial model for the response variables of *Brassica oleracea* (BO).

Source	df	ABTS (%)			DPPH• (%)			TAC (mg Cy3G/100 g FW)		
		Coefficient	Sum of squares	*p*-Value	Coefficient	Sum of squares	*p*-Value	Coefficient	Sum of squares	*p*-Value
Model	5	47.94	89.00	<0.0001	42.00	93.46	<0.0001	104.54	106.46	<0.0001
Linear										
A	1	0.8417	4.25	0.0004	0.8183	4.02	0.0017	0.7100	3.02	0.0188
B	1	−0.7817	3.67	0.0007	−0.9117	4.99	0.0009	−0.9133	5.01	0.0058
Quadratic										
AB	1	−1.01	4.12	0.0005	−1.05	4.41	0.0013	−1.2	5.88	0.0038
Interaction										
A^2	1	−2.44	16.51	<0.0001	−2.33	14.99	<0.0001	−2.73	20.58	<0.0001
B^2	1	−3.39	31.83	<0.0001	−3.60	35.79	<0.0001	−3.68	37.40	<0.0001
Residual	7		0.7602			1.16			2.29	
Lack of fit	3		0.4684	0.578		0.7408	0.2137		0.8677	0.5493
Pure error	4		0.2918			0.4203			1.42	
Total	12		89.76			94.62			108.75	
Adj. R^2		0.9855			0.9790			0.9639		
Pred. R^2		0.9550			0.9400			0.9160		
C.V. %		0.7283			1.04			0.5630		

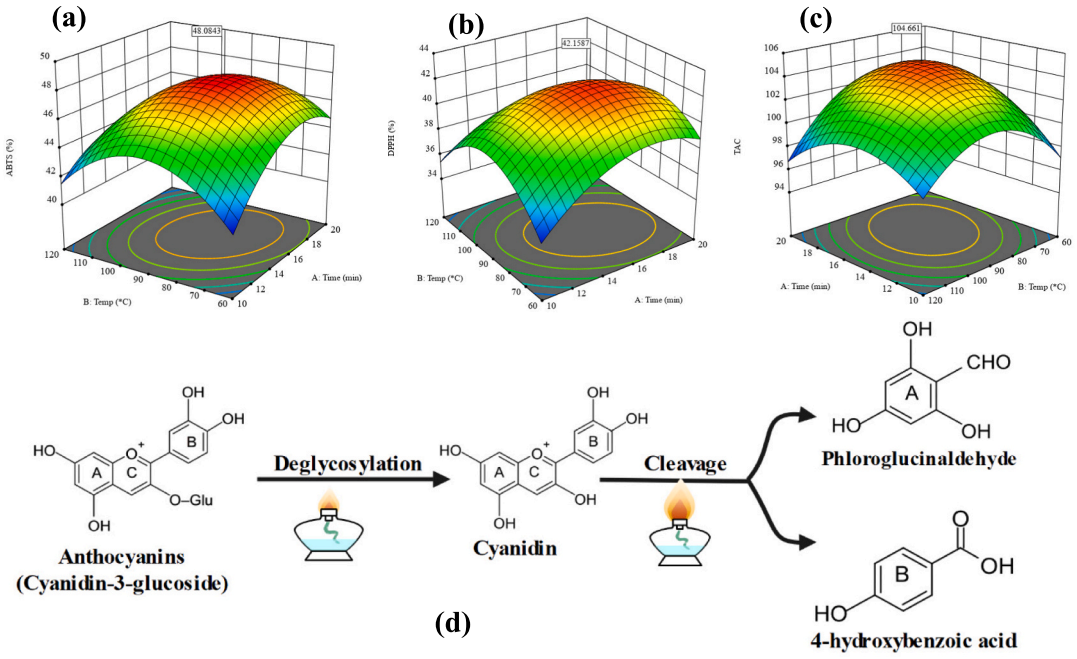

Fig. 1. (a) 3D surface plots for ABTS (%), (b) 3D surface plots for DPPH• (%), (c) 3D surface plots for TAC (mg Cy3G/100 g FW) of BO in the function of extraction temperature (°C) and extraction time (min), (d) mechanism of thermal degradation of anthocyanins.

3.2. Characterization of BO-CDs

3.2.1. Photoluminescence & UV–Vis properties of BO-CDs

UV–Vis and fluorescence spectrophotometry results demonstrated that synthesized BO-CDs were excellent photon harvesters which might be due to the light absorption of the conjugated electrons in the sp2 atomic framework, especially in short wavelength areas [28]. As depicted in Fig. 2a, BO-CDs showed strong optical absorption at 370 nm, which was mainly derived from the electron transition from $\pi \rightarrow \pi^*$ of the C—C bonds and $n \rightarrow \pi^*$ of the C—O bonds [19] at the edges of BO-CDs with a tail spreading into the visible region. This UV-absorbance property of BO-CDs positioned them as active candidatures for the development of UV-barrier active packaging films.

Photoluminescence (PL) spectrometry, often called excitation-dependent fluorescence emission, is used to characterize CDs [29]. The fluorescence spectrum of the BO-CDs showed the strongest fluorescence emission at 486 nm with an excitation wavelength of 370 nm. The fluorescence emission also shifted to a higher wavelength as the excitation wavelength increased (Fig. 2b), indicating excitation-dependent emission of BO-CDs [30]. The BO-CD solution showed illuminating blue scattering emission under UV (365 nm) while appearing completely transparent under normal light (Fig. 2a). It is well-documented that CDs (5–10 nm in size) are strong photon emitters under UV excitation [18,28,29]. Similar results have been observed for carbon dots (CDs) synthesized using citric acid [31].

3.2.2. FTIR, XPS, TEM, and antibacterial analysis of BO-CDs

FTIR spectrometry is a non-destructive and real-time analytical method enabling the characterization of the functional groups of the carbon dots [31]. The signal peaks at 3301, 2962, 1579, 1384, and 1109 cm^{-1} in the FTIR spectra (Fig. 3a) were assigned to O—H, C—H, C═C [19], N—H, and C═O, respectively [31]. These observations confirmed nitrogen structure (N—H groups) in the synthesized CDs. Results indicated that the synthesized BO-CDs were self-functionalized with hydroxyl, carbonyl, and amino groups, which impart excellent aqueous solubility and biocompatibility for further applications.

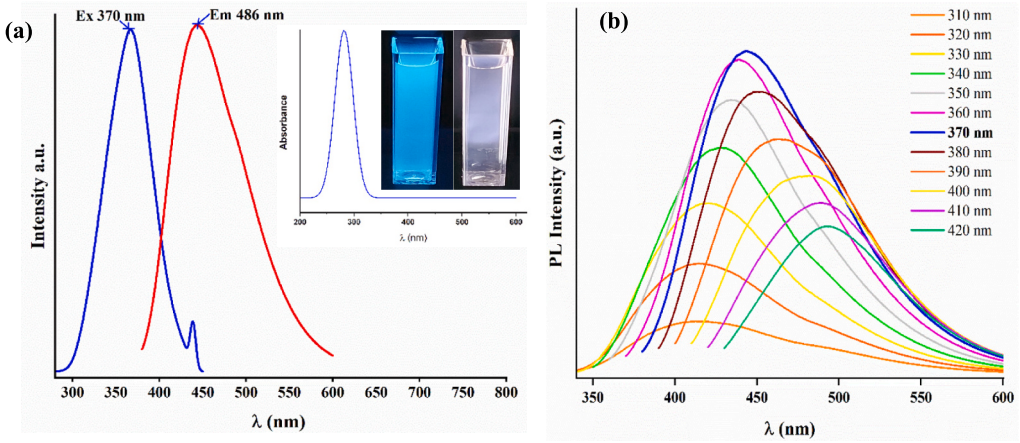

Fig. 2. (a) UV–Vis spectrum (b) Photo-luminance spectrum of BO-CDs.

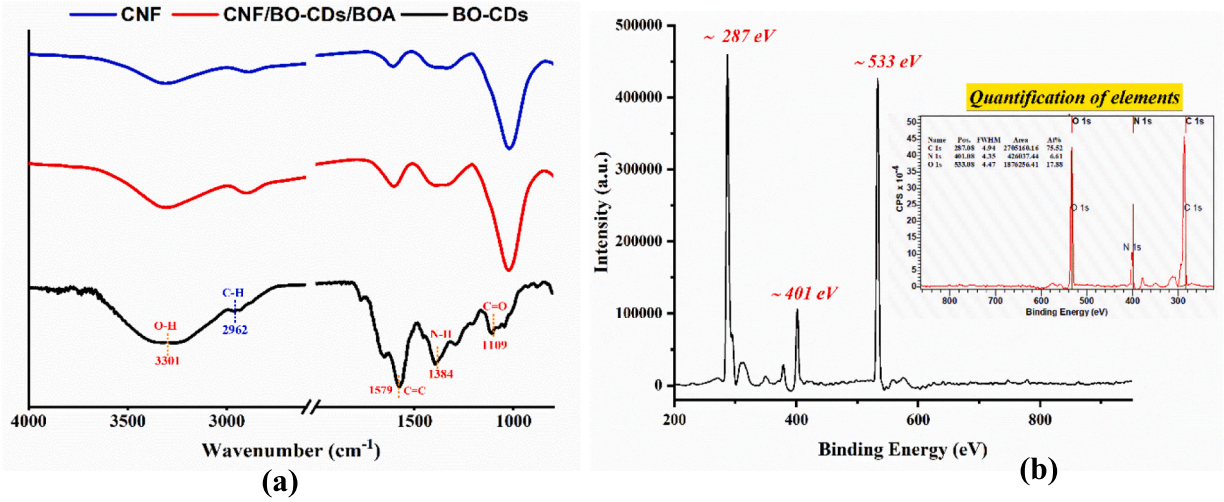

Fig. 3. (a) FT-IR spectra of neat CNF, CNF/BO-CDs/BOA, and BO-CDs (b) XPS analysis of BO-CDs.

In addition, the elemental composition and surface state of BO-CD were analyzed by XPS spectroscopy (Fig. 3b). Three peaks at 533, 401, and 287 eV indicated the presence of O 1s, N 1s, and C 1s elements in the BO-CDs, respectively [32]. The presence of nitrogen (pyrrolic N) was attributed to proteins, amino acids, and vitamins of the BO [13]. Moreover, the elemental analysis results revealed that the BO-CDs comprised 75.52 wt% of C, 6.61 wt% of N, and 17.88 wt% of O (Fig. 3b), verifying several functional surface groups on the BO-CDs, including carboxyl, hydroxyl, and amino groups. The XPS results are in good agreement with that of FTIR.

Transmission electron microscopy (TEM) studies showed spherical (2.4–4.0 nm) and evenly distributed carbon dots (Fig. S1). Such distribution might be due to polar-polar interaction between different hydrophilic functional groups on the surface [18]. The particle size distribution histograms indicated the diameters ranged from 2.4 to 4.0 nm and an average diameter of 3.2 nm (Fig. S1).

The sensitivity of *E. coli* (Gram-negative) and *L. monocytogenes* (Gram-positive) strains to BO-CDs was measured using an agar well diffusion assay (Fig. S2). The results indicated that synthesized BO-CDs exhibited a strong zone of inhibition against *L. monocytogenes* (~21 mm) compared to *E. coli* (~3 mm) at 100 μL concentration. The antibacterial activity of the synthesized BO-CD can be explained by the electrostatic surface charge state of the CD attracting microbial cells [33–35]. Light-induced excitation associated with $\pi \rightarrow \pi^*$ (Fig. 2a) in the carbon core of the CD induces the formation of highly reactive singlet oxygen species (ROS) [33,34]. ROS plays an important role in the antibacterial effect of CDs [34]. By photoexcitation, electron-hole pairs form in the carbon core of CDs and are localized at the surface defects of the bacterial cell membrane. Generation of electron-hole pairs and their transfer to the associated proximal species can produce radical species ($^{\bullet}OH$ and $O_2^{\bullet-}$), which could impose oxidative damages on bacterial cells, such as morphological changes of the cell membrane, cytoplasmic leakage, and DNA impairment [33–35].

These promising findings shed light on the antibacterial abilities of synthesized BO-CDs, potentially providing ground for the use as an antibacterial agent for food packaging films. The excellent antibacterial effect of *Brassica oleracea* extract is well known [12,14].

3.2.3. Antioxidant activity of BO-CDs

$ABTS^{\bullet+}$ and $DPPH^{\bullet}$ scavenging activity are primarily used to evaluate the radical scavenging or antioxidant activity [16]. Fig. S3 shows the antioxidant activity of BO-CDs in terms of $ABTS^{\bullet+}$ and $DPPH^{\bullet}$ scavenging assay. Radical scavenging activity gradually increased with the increasing concentration (dose-dependent manner) of BO-CDs from 12.5 to 100 μg/mL (Fig. S3). The EC_{50} value (effective concentration required to inhibit 50 % of free radicals) of the BO-CDs was 22.19 and 54.93 μg/μL for $ABTS^{\bullet+}$ and $DPPH^{\bullet}$ assays, respectively. In this study, the color of the $DPPH^{\bullet}$ solution (deep violet) was changed to light yellow owing to

the synthesis of the corresponding hydrazine DPPH2• [36], which might be attributed to the pairing of a lone pair of electrons of a DPPH• radical with a cation or H^+ of synthesized BO-CDs [13]. These results confirmed that synthesized BO-CDs would further expand their role as a natural and potent antioxidant agent for food packaging applications.

3.3. Characterization and properties of the films

3.3.1. FTIR, TGA, and SEM analysis

The prepared CNF-based films were free-standing and flexible. Fourier-transform infrared spectroscopy (FTIR) spectra (Fig. 3a) of the neat CNF and CNF/BO-CDs/BOA films showed broad peaks near 3310–3314 cm^{-1} were attributed to the O—H stretching vibration (intermolecular/intramolecular) and H-bonding [36]. The peaks at 2892–2903 cm^{-1} were attributed to C—H stretching vibration [31]. The peak at 1601–1604 and 1391–1393 cm^{-1} was ascribed to C═C stretching (aromatic structure) and -NH/amide-II (carbonyl stretching) stretch vibrations, respectively [31,36]. The firm peaks at 1021–1024 cm^{-1} were due to the C═O stretching vibrations contributed by CNF polymer matrices [19]. After impregnating BO-CDs/BOA into the CNF matrix, little peak intensity and position change were found in the CD-doped film. Overall, however, the FTIR patterns resembled the neat CNF. The slight change in the IR spectrum after infusing the BO-CDs/BOA was due to the overlapping C—H, OH, C═C, and C═O stretching vibration in almost the same IR region. The reason for the negligible change in the IR spectra could be due to similar elemental compositions and surface functionalities for the materials used (CNF, BO-CD, and BOA). Therefore, the intensity of the peak obtained in the spectrum of the CD-doped film remains the same, with a slight shift in the frequency domain, suggesting the suitability of BO-CD/BOA for the CNF-polymer matrix (Fig. 3a).

The scanning electron microscopy (SEM) image of the neat CNF film appeared smooth, intact, and curved with wavy clumps (Fig. 4a). The incorporation of BO-CDs/BOA produced a much smoother surface than pure CNF and did not compromise the surface appearance as there were no surface cracks, cavities, and lumps, indicating that BO-CDs/BOA had good compatibility with CNF blends. From the observation of the SEM images, it can be suggested that the hydrophilic nature of BO-CDs/BOA and the formation of hydrogen bonds between the surface functional groups may be responsible for the uniform mixing of CD and CNF polymer matrices [18]. In one report, the enrichment of red cabbage extract with chitosan/chitin nanocrystal composites resulted in smoother and denser cross-sectional surfaces, suggesting that the added anthocyanins had good compatibility and embedding properties in the interspaces of the polymer composites [1]. Improved uniformity/adhesion can be attributed to the following factors: First, the extracted BOA made the aqueous extraction solvent more polar [6,12,13]. Second, the added BO-CD and CNF matrices can form intermolecular hydrogen bonds, resulting in dense and cohesive films [13].

Fig. 4b depicts the thermo-gravimetry (TGA), and Fig. S4b shows the derivative thermo-gravimetry (DTGA) of the neat CNF and developed indicator films. The TGA slope of pure CNF showed four zones of weight loss compared to three in developed indicator films. The first weight loss of 6 % occurred till 58 °C for CNF and 4.9 % till 66 °C for indicator films,

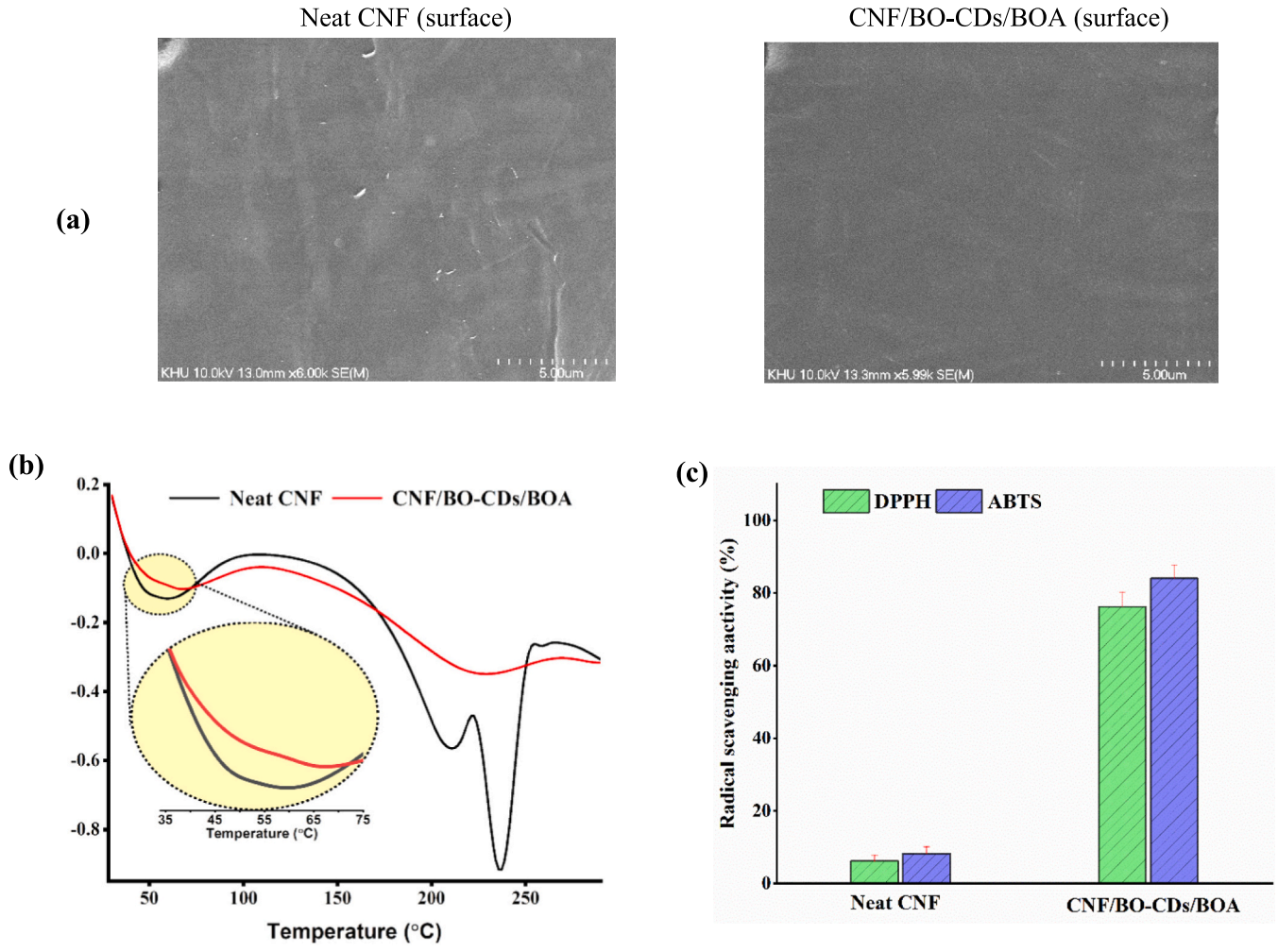

Fig. 4. (a) FE-SEM (surface); (b) TGA thermograms, and (c) antioxidant activity of the neat CNF and CNF/BO-CDs/BOA films.

signifying >12 % temperature tolerance of CNF/BO-CDs/BOA films than the neat CNF film. This weight loss was due to the moisture evaporation in the film [37]. The WVP studies support these findings, indicating that decreased WVP properties of CNF/BO-CDs/BOA might delay the release of thermal degradation products compared to neat polymer films. Roy and Rhim also found a similar effect of shikonin on the thermal stability of cellulose-based color indicator films [4].

The second prominent thermal degradation was noticed around 236–286 °C, with maximum weight loss (32 %–38 %) caused by glycerol and polymer backbone decomposition (Fig. 4b). Contrary to previous findings, the addition of anthocyanins was found to result in significant weight loss of the polymer film [14]. In contrast, the addition of BO anthocyanins (6 % v/v) greatly improved the thermal stability of the developed indicator films. Improved thermal stability could be attributable to the synergistic cross-linking effect of BOA/BO-CDs (justified by SEM), hindering thermal degradation. The final (char) stage resulted in 14.34 % and 18.44 % mass loss of neat CNF and indicator films (Fig. S4b) due to dehydroxylation and complete depolymerization of the polymer matrix. These results are consistent with those reported by Pereira et al. [6].

3.3.2. Physicochemical, antioxidant, and optical properties of the films

The thickness of the films ranged from 26.60 μm to 34.88 μm for the neat CNF and CNF/BO-CDs/BOA films, respectively (Table S4). The increased thickness of the composite film was due to the addition of solid-dense content [37]. The mechanical properties of the neat CNF and CNF/BO-CDs/BOA films are shown in Table S3. The tensile strength of the CNF film increased with the addition of BO-CD and BOA ($p > 0.05$). This increase may be due to a corresponding increase in interfacial interactions, such as H-bonds between the CNF matrix and BO-CD/BOA [11]. However, the addition of anthocyanin and CD did not significantly change the elongation at the break of the developed film. Other researchers reported similar results [11], where shikonin increases the tensile strength but does not significantly increase the elongation at breakage of cellulose-nanofiber-based packaging films.

The water contact angle (WCA) indicates a film's surface hydrophobicity or hydrophilicity. Biopolymer films are considered hydrophilic when the WCA is <65° [8]. The WCA of CNF (37.3 ± 3.9°) and CNF/BO-CDs/BOA (48.3 ± 2.9°) films were <65°, indicating the films are highly hydrophilic. The addition of BOA and BO-CDs to the CNF matrix resulted in a significant ($p > 0.05$) increase in the WCA, leading to increased surface hydrophobicity, due to the improved synergistic cross-linking firmness of the films as observed in the SEM results [11].

The WVP signifies the barrier attributes of the film against water vapor, and reduced WVP is a desirable attribute for packaging films for better outcomes [19]. As shown in Table S4, the WVP of developed indicator films decreased ($p < 0.05$) after the dual-doping of CNF by BOA and BO-CDs in contrast to pure CNF films. These results may be related to the bulky aromatic rings in the skeleton structures of BOA that densified the microstructural networks of films and diminished the binding affinity towards water molecules [11]. Furthermore, the unique molecular geometry of BO-CDs could also promote a cross-net effect in CNF films, which restricted the movement of water vapor molecules, thereby lowering WVP [13]. The addition of BOA and BO-CD significantly ($p < 0.05$) improved the WVP of CNF-based nanocomposite films.

The results of instrumental color analysis of the CNF and CNF/BO-CDs/BOA films are also shown in Table S4. As projected from the UV–Vis spectrum (Fig. S4a), the control film showed moderate L^* values and low a^* and b^* values, indicating that the film was transparent/colorless [11]. While the incorporation of BOA/BO-CDs, increased the L^*, b^*, and a^* values of the films compared to the neat CNF film, resulting in visible red-purplish color. The total color variance (ΔE) of the films also increased significantly ($p < 0.05$) when incorporated with BOA+BO-CDs (>20) than CNF films (<8); this was due to the incorporation of purplish-red BOA and brown-red BO-CDs.

In recent years, UV shielding films have garnered much attention. Exposure to UV light leads to nutrient loss, discoloration, off-flavors, and oxidative deterioration of packaged foods [19,38]. As shown in Fig. S4 (a), UV-transmission and visible light were ($p < 0.05$) reduced by the inclusion of BOA and BO-CDs-in CNF polymer matrix. These results can be justified in two ways. First, added BOA (6 %) has anthocyanin-rich aromatic rings and flavonoids, which can act as a powerful UV blocker [12]. Secondly, added BO-CDs exhibited strong UV absorbance ability (Fig. 2a). Our results suggested that the developed films can be applied as a potential UV-light barrier film apart from their intelligent abilities in food packaging systems.

Intelligent food packaging materials with radical scavenging abilities protect foods from damage and oxidative degradation. The antioxidant properties in terms of $ABTS^{\bullet+}$ and DPPH radical scavenging activities of the CNF-based films are shown in Fig. 4c. The fortification of the CNF matrix with antioxidant-rich BOA and antibacterial/antioxidant (Fig. S3a and b) rich BO-CDs resulted in obvious inherent increased $ABTS^{\bullet+}$ and $DPPH^{\bullet}$ scavenging abilities of the CNF/BO-C59Ds/BOA films as compared to the neat CNF film.

3.3.3. Simulation test

Experimental analysis (Fig. 5a) shows the response of RSM-optimized BOA extracts at different pH levels. BOA showed noticeable and significant responses and differences at the various pH levels studied. Muscle food deterioration produces a variety of volatile chemicals such as amines, sulfides, ammonia, and others [22]. Among them, volatile nitrogen substances, particularly ammonia, cause the pH increase in muscle foods. A simulation food deterioration study using ammonia and acetic acid (AA) was conducted to evaluate the sensitivity of developed CNF/BO-CDs/BOA films. The sensitivity concerning instrumental color variations (L^*, a^*, and b^*) of films to NH_3 and AA are shown in Fig. 5c. After 30 min exposure to NH_3 and AA, films showed significant color variations. The CNF/BO-CDs/BOA films without exposure to NH_3/AA showed a brownish-black hue. L^* values were higher for the control films (35.85), followed by NH_3-exposed films, and lowest for AA-exposed films (31.92). The film exposed to AA had the highest redness/a* value (3.47), followed by the control film (2.45), and the film exposed to NH_3 had the lowest. These results indicate that the acidic environment results in a significant color change from brown-black to reddish-brown, readily visible to the naked eye.

Compared to the control and AA films, the NH_3 exposed films showed significantly higher yellowness/b^* values (5.23), indicating a more pronounced yellowish-opaque color shift. The volatile NH_3 interacted with H_2O in the film to generate NH_3:H_2O, which then hydrolyzed to release NH_4^+ and OH^- [1], which triggered the pH increase, resulting in a color change of the films. Overall, the developed CNF/BO-CDs/BOA films could monitor and signal the presence of volatile ammonia and acidity inside the package. Developed CNF/BO-CDs/BOA films displayed visible color variations in response to treatment with pH 2 to 12 buffer solutions, as shown in Fig. 5b, verifying their potent application for the halochromic indicator films development.

3.4. In vivo studies

Broadly, techniques for assessing muscle food for freshness or deterioration fall into destructive and non-destructive categories [2,15]. Destructive methods require preparation and manipulation of the sample resulting in time-consuming and expensive methods. Non-destructive methods employ a variety of approaches that do not need extensive sample preparation and thus provide quick results without modifications caused by the various preparation steps [29].

An attempt was made to design a non-destructive, simple, and efficient system using a developed CNF/BO-CDs/BOA film indicator for evaluating real-time monitoring of quality changes in an *in vivo* model system, *viz.* minced pork, fish, and shrimps.

In this study, the pH, extract release volume (ERV), total color change (ΔE), and consumer sensory scores (overall acceptability) were

(a)

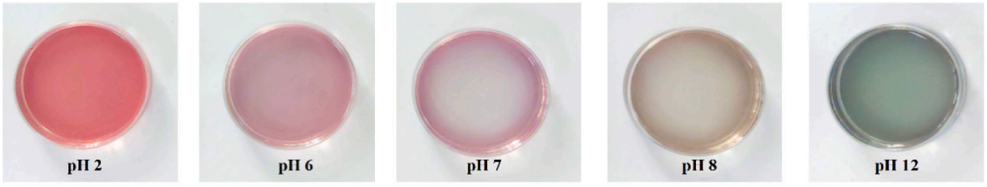

(b)

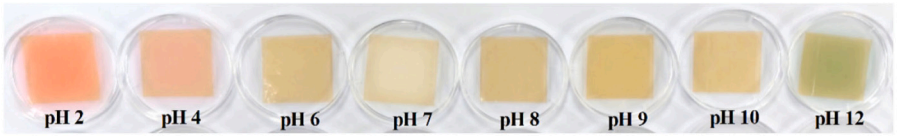

(c)

Color values	Control indicator films	NH_3 exposure	Acetic acid exposure
L^*	35.85±2.14	33.21±1.05	31.92±2.18
a^*	2.45±0.47	1.66±0.89	3.47±0.77
b^*	3.41±0.95	5.23±1.08	2.94±0.84
Photo images of the indicator films			

Fig. 5. (a) Halochromic color response of optimized BOA at different pH, (b) Halochromic color response of CNF/BO-CDs/BOA indicator films, (c) simulation results of CNF/BO-CDs/BOA with NH_3 and acetic acid exposure.

demonstrated as the quality index to monitor the freshness of *in vivo* food models over the storage period of 48 h at 25 °C (Fig. 6a). The intricacies of food storage quality indexes with color attributes of the indicator films have been attempted. The pH of all the studied food models increased significantly with an increase in storage period of 48 h, a more pronounced increase was reported in fish samples from 5.81 ± 0.01 to 7.09 ± 0.01 followed by minced pork from 5.85 ± 0.21 to 6.81 ± 0.02 and least in shrimp samples from 6.27 ± 0.01 to 7.20 ± 0.08 (Fig. 6a). It has been documented that pork is graded as fresh with pH of 5.18 to 6.12 and sub-fresh (6.13 and 6.16) [38].

Previous studies reported that a pH value of approximately >7.0 (fish/shrimp) and >6.8 (pork) indicated the onset of deterioration [2,15,38]. The increases in pH during storage are due to the formation of spoilage compounds, including ammonia, dimethylammonium, sugar complexes, and trimethylamine, leading to the decomposition of protein and lipids [22,39,40]. A similar color change was observed in a study that monitored the freshness of chicken breast meat using curcumin-containing chitosan/PEO nanofibers [9].

The extract-release volume (ERV) test is a reliable and quick predictor of microbial deterioration of meat and has also been shown to have an inverse relationship with the bacterial population of muscle tissues [41]. It is assumed that meat should have an ERV value greater than or equal to 25 mL to be graded within the acceptable range [42].

The ERV values for minced pork, fish, and shrimp were within the permissible range for the first 24 h of storage, indicating the samples were in an acceptable range (Fig. 6a). At 48 h of storage, ERV decreased significantly (<25) as spoilage progressed and bacterial population increased.

Consumers evaluate the quality of meat and meat products using three sensory factors: texture, flavor, and appearance [16,22]. The appearance of a product is the most important characteristic that influences a consumer's purchase decision. The consumer panel consisting of eleven semi-trained members conducted a sensory evaluation of stored *in vivo* food models at a regular interval of 12 h. Fig. 6a shows that the OA score of fresh pork, fish, and shrimp (0 h) was 4.98, 4.93, and 4.98, respectively. After storage for 24 h, it decreased to 2.50, 2.52, and 2.69 for pork, fish, and shrimp, respectively. All the food models were within the acceptable range of OA (2.5) till 24 h of storage [16]. Finally, the decline in OA (<2.5) with the progression of storage (48 h) leads to sensory rejection (Fig. 6c).

The color attributes of film containing 6 % BOA anthocyanin changed steadily with increasing pH, resulting from purple-red colors at 0 h to yellowish-white or colorless at 48 h (Fig. 6b). The total color difference (ΔE) at 0 h of storage was 51.15, 51.65, and 52.38 for pork, fish, and shrimp indicators, respectively. After 48 h of storage, the ΔE changed to 63.73, 62.29, and 62.08 for pork, fish, and shrimp, respectively. These color changes are expected to make the developed indicator film intelligently respond to the real-time monitoring of quality changes in the food models.

Anthocyanins could exist in various chemical forms depending on the pH, temperature, and enzyme reactions [27]. Due to their instability, the pH-dependent color response of anthocyanins is more pronounced in the alkaline province [12]. At pH values 5 to 7, the anthocyanins are degraded to flavylium cation, anhydrous quinoidal base, colorless carbinol base, and the pale yellow chalcone [11] (Fig. 6d). Later, two played an important role in changing red-purple anthocyanins to yellowish/colorless cations, which was evident from our research findings [1,11].

With the progression of the storage period, bacterial decomposition and degradation of muscle led to the production of various enzymatic products like glycosidases, peroxidases, and alkaline chemicals. The most common enzymes that degrade anthocyanins are anthocyanins

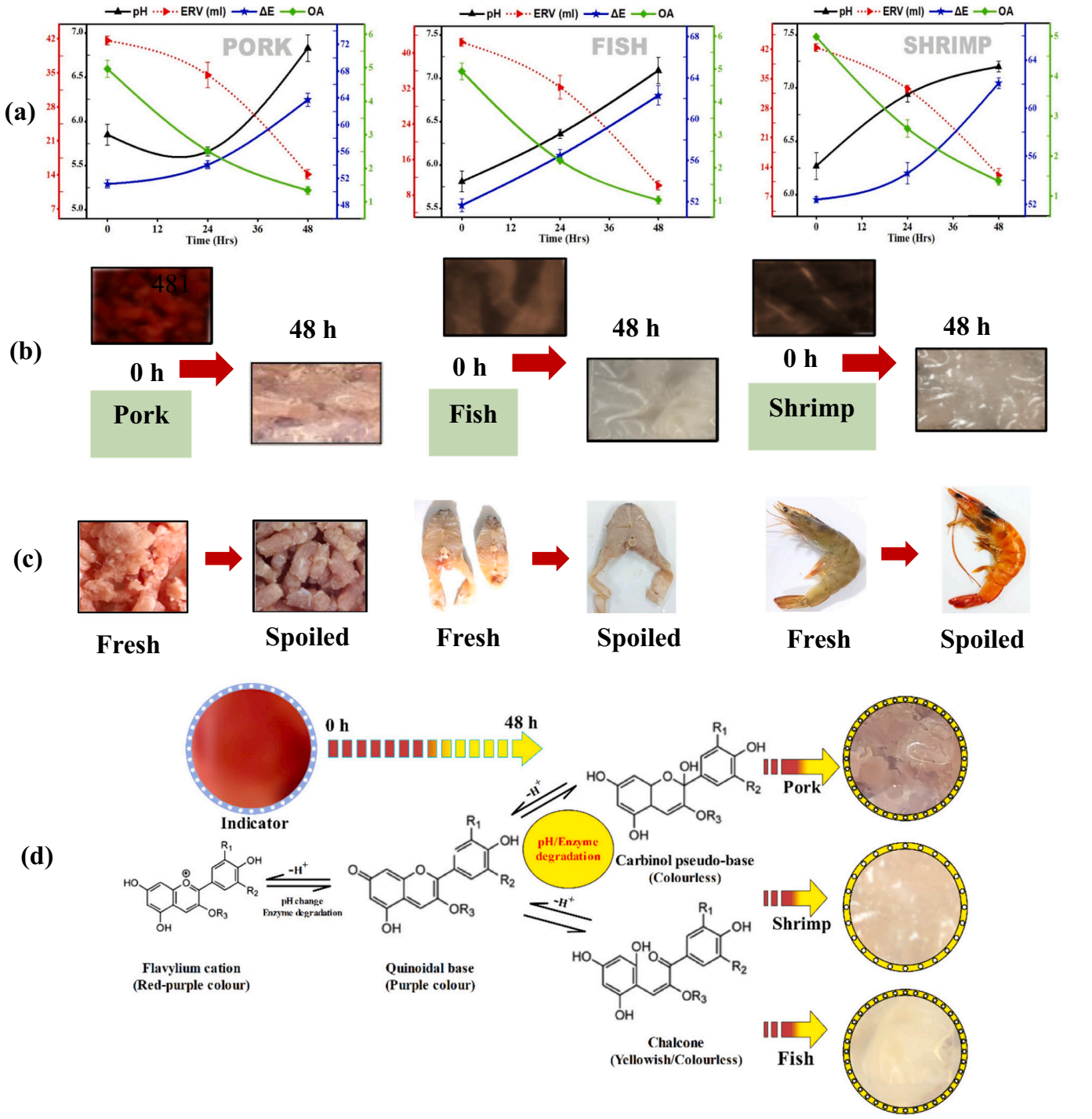

Fig. 6. (a) Quality appraisal of fish, pork, and shrimp storage studies at 25 °C for 48 h, (b) color response of CNF/BO-CDs/BOA indicator films, (c) photographs of stored fish, pork, and shrimp (at 0 h and 48 h), (d) mechanism of pH/enzyme-dependent color changes of anthocyanins during 48 h storage.

(glycosidases/peroxidases) [12,27,43]. It is worth noting that glycosidases directly affect anthocyanin's stability (Fig. 6d), leading to substantial color change [5,11,12].

Compared to pure CNF films, developed CNF/BO-CDs/BOA films withstand without any structural integrity loss inside the storage box, which might be ascribed to the antimicrobial and antioxidant scavenging abilities of infused BO-CDs in intelligent indicator films, making them nano-multifunctional films, proving their contention for real-time monitoring of minced pork, fish, and shrimp.

4. Conclusions

An optimized Response Surface Methodology (RSM) with one-step central-composite modeling depicted the higher total anthocyanin contents (104.66 mg Cy3G/100 g FW), (48.08 %) $ABTS^{\bullet+}$ and (42.15 %) $DPPH^{\bullet}$ scavenging activity at an extraction time of 16.00 min and temperature of 85.45 °C for yielding bioactive *Brassica oleracea* anthocyanins (BOA). BO-based bio-waste was successfully converted to synthesize highly fluorescent, UV-absorbent, and antimicrobial, antioxidant-rich carbon quantum dots (BO-CDs) using a green

hydrothermal (180 °C/7 h) approach for active packaging applications. Incorporating optimized BOA (6 %) and BO-CDs (1.5 %) in the CNF matrix showed a uniform morphology (SEM) and improved polymeric matrix distribution/functional groups (FTIR, XPS) with >12 % improved thermal stability at 65 °C. Obtained results demonstrated a significant improvement of about 25.70 % in WCA, 38.83 % in WVP, >189 % in UV-barrier, and 164 % in the antioxidant properties of the indicator films as compared to the neat CNF film. *In vivo* storage model studies revealed that the developed films function as active films and monitor the real-time freshness of pork/fish/shrimp by quantifiable and intelligible visual changes. As raw materials used for fabricating indicator films were non-toxic and biodegradable, these films can be used as safe and eco-friendly freshness indicators for reducing food waste and extending the storage life of food.

Declaration of competing interest

The authors declare that they have no known competing financial interests or personal relationships that could have appeared to influence the work reported in this paper.

Data availability

Data will be made available on request.

Acknowledgment

The work was executed under the financial assistance for the International training provided by the Indian Council of Agricultural Research, New Delhi, India through the National Agricultural Higher Education Project (IDP-NAHEP) running at Guru Angad Dev Veterinary and Animal Sciences University, Ludhiana, Punjab (INDIA). This work was supported by the National Research Foundation of Korea (NRF) grant funded by the Korean government (MSIT) (2022R1A2B5B02001422).

Appendix A. Supplementary data

Supplementary data to this article can be found online at https://doi.org/10.1016/j.ijbiomac.2023.123567.

References

[1] M. Chen, T. Yan, J. Huang, Y. Zhou, Y. Hu, Fabrication of halochromic smart films by immobilizing red cabbage anthocyanins into chitosan/oxidized-chitin nanocrystals composites for real-time hairtail and shrimp freshness monitoring, Int. J. Biol. Macromol. 179 (2021) 90–100, https://doi.org/10.1016/j.ijbiomac.2021.02.170.

[2] J.-H. Cheng, Q. Dai, D.-W. Sun, X.-A. Zeng, D. Liu, H.-B. Pu, Applications of non-destructive spectroscopic techniques for fish quality and safety evaluation and inspection, Trends Food Sci. Technol. 34 (2013) 18–31, https://doi.org/10.1016/j.tifs.2013.08.005.

[3] D. Yun, Y. He, H. Zhu, Y. Hui, C. Li, D. Chen, J. Liu, Smart packaging films based on locust bean gum, polyvinyl alcohol, the crude extract of Loropetalum chinense var. rubrum petals and its purified fractions, Int. J. Biol. Macromol. 205 (2022) 141–153, https://doi.org/10.1016/j.ijbiomac.2022.02.068.

[4] S. Roy, H.-J. Kim, J.-W. Rhim, Effect of blended colorants of anthocyanin and shikonin on carboxymethyl cellulose/agar-based smart packaging film, Int. J. Biol. Macromol. 183 (2021) 305–315, https://doi.org/10.1016/j.ijbiomac.2021.04.162.

[5] X. Yao, Y. Qin, M. Zhang, J. Zhang, C. Qian, J. Liu, Development of active and smart packaging films based on starch, polyvinyl alcohol, and betacyanins from different plant sources, Int. J. Biol. Macromol. 183 (2021) 358–368, https://doi.org/10.1016/j.ijbiomac.2021.04.152.

[6] V.A. Pereira, I.N.Q. de Arruda, R. Stefani, Active chitosan/PVA films with anthocyanins from Brassica oleraceae (red cabbage) as time-temperature indicators for application in intelligent food packaging, Food Hydrocoll. 43 (2015) 180–188, https://doi.org/10.1016/j.foodhyd.2014.05.014.

[7] W. Li, W. Sun, L. Jia, Y. Dong, L. Wu, M.D.A. Saldaña, W. Sun, Poly-l-lactic acid (PLLA)/anthocyanin nanofiber color indicator film for headspace detection of low-level bacterial concentration, Int. J. Biol. Macromol. 215 (2022) 123–131, https://doi.org/10.1016/j.ijbiomac.2022.06.034.

[8] P. Ezati, Y.-J. Bang, J.W. Rhim, Preparation of a shikonin-based pH-sensitive color indicator for monitoring the freshness of fish and pork, Food Chem. 337 (2021), 127995, https://doi.org/10.1016/j.foodchem.2020.127995.

[9] E. Yildiz, G. Sumnu, L.N. Kahyaoglu, Monitoring freshness of chicken breast by using natural halochromic curcumin loaded chitosan/PEO nanofibers as an intelligent package, Int. J. Biol. Macromol. 170 (2021) 437–446, https://doi.org/10.1016/j.ijbiomac.2020.12.160.

[10] K. Zhang, T.-S. Huang, H. Yan, X. Hu, T. Ren, Novel pH-sensitive films based on starch/polyvinyl alcohol and food anthocyanins as a visual indicator of shrimp deterioration, Int. J. Biol. Macromol. 145 (2020) 768–776, https://doi.org/10.1016/j.ijbiomac.2019.12.159.

[11] S. Roy, J.W. Rhim, Fabrication of cellulose nanofiber-based functional color indicator film incorporated with shikonin extracted from Lithospermum erythrorhizon root, Food Hydrocoll. 114 (2021), 106566, https://doi.org/10.1016/j.foodhyd.2020.106566.

[12] N. Ghareaghajlou, S. Hallaj-Nezhadi, Z. Ghasempour, Red cabbage anthocyanins: stability, extraction, biological activities and applications in food systems, Food Chem. 365 (2021), 130482, https://doi.org/10.1016/j.foodchem.2021.130482.

[13] N. Sharma, G.S. Das, K. Yun, Green synthesis of multipurpose carbon quantum dots from red cabbage and estimation of their antioxidant potential and bio-labeling activity, Appl. Microbiol. Biotechnol. 104 (2020) 7187–7200, https://doi.org/10.1007/s00253-020-10726-5.

[14] M.C. Silva-Pereira, J.A. Teixeira, V.A. Pereira-Júnior, R. Stefani, Chitosan/corn starch blend films with extract from brassica oleraceae (red cabbage) as a visual indicator of fish deterioration, LWT Food Sci. Technol. 61 (2015) 258–262, https://doi.org/10.1016/j.lwt.2014.11.041.

[15] M. Alizadeh Sani, M. Tavassoli, S.A. Salim, M. Azizi-lalabadi, D.J. McClements, Development of green halochromic smart and active packaging materials: TiO2 nanoparticle- and anthocyanin-loaded gelatin/κ-carrageenan films, Food Hydrocoll. 124 (2022), 107324, https://doi.org/10.1016/j.foodhyd.2021.107324.

[16] N.S. Jagtap, R.V. Wagh, M.K. Chatli, P. Kumar, O.P. Malav, N. Mehta, Optimization of extraction protocol for Carica papaya L. to obtain phenolic rich phyto-extract with prospective application in chevon emulsion system, J. Food Sci. Technol. 56 (2019) 71–82, https://doi.org/10.1007/s13197-018-3456-8.

[17] D. Hoehn, I. Vázquez-Rowe, R. Kahhat, M. Margallo, J. Laso, A. Fernández-Ríos, I. Ruiz-Salmón, R. Aldaco, A critical review on food loss and waste quantification approaches: is there a need to develop alternatives beyond the currently widespread pathways? Resour. Conserv. Recycl. 188 (2023), 106671 https://doi.org/10.1016/j.resconrec.2022.106671.

[18] M. Moradi, R. Molaei, S.A. Kousheh, J.T. Guimarães, D.J. McClements, Carbon dots synthesized from microorganisms and food by-products: active and smart food packaging applications, Crit. Rev. Food Sci. Nutr. (2021) 1–17, https://doi.org/10.1080/10408398.2021.2015283.

[19] P. Ezati, J.W. Rhim, R. Molaei, R. Priyadarshi, S. Han, Cellulose nanofiber-based coating film integrated with nitrogen-functionalized carbon dots for active packaging applications of fresh fruit, Postharvest Biol. Technol. 186 (2022), 111845, https://doi.org/10.1016/j.postharvbio.2022.111845.

[20] J.P. Malavika, C. Shobana, M. Ragupathi, P. Kumar, Y.S. Lee, M. Govarthanan, R. K. Selvan, A sustainable green synthesis of functionalized biocompatible carbon quantum dots from Aloe barbadensis Miller and its multifunctional applications, Environ. Res. 200 (2021), 111414, https://doi.org/10.1016/j.envres.2021.111414.

[21] D. Rawtani, P.K. Rao, C.M. Hussain, Recent advances in analytical, bioanalytical and miscellaneous applications of green nanomaterial, TrAC Trends Anal. Chem. 133 (2020), 116109, https://doi.org/10.1016/j.trac.2020.116109.

[22] R.V. Wagh, M.K. Chatli, M. Ruusunen, E. Puolanne, P. Ertbjerg, Effect of various phyto-extracts on physico-chemical, color, and oxidative stability of pork frankfurters, Asian-Australas. J. Anim. Sci. 28 (2015) 1178, https://doi.org/10.5713/AJAS.14.0752.

[23] Y.-Z. Tang, Z.-Q. Liu, Free-radical-scavenging effect of carbazole derivatives on DPPH and ABTS radicals, J. Am. Oil Chem. Soc. 84 (2007) 1095–1100, https://doi.org/10.1007/s11746-007-1149-y.

[24] A. Antony, M. Farid, Effect of temperatures on polyphenols during extraction, Appl. Sci. 12 (2022) 2107, https://doi.org/10.3390/app12042107.

[25] E. Conde, C. Cara, A. Moure, E. Ruiz, E. Castro, H. Domínguez, Antioxidant activity of the phenolic compounds released by hydrothermal treatments of olive tree pruning, Food Chem. 114 (2009) 806–812, https://doi.org/10.1016/j.foodchem.2008.10.017.

[26] A. Patras, P. Nigel, C. Brunton, B.K.Tiwari O'Donnell, Effect of thermal processing on anthocyanin stability in foods; mechanisms and kinetics of degradation, Trends Food Sci. Technol. 21 (2010) 3–11, https://doi.org/10.1016/j.tifs.2009.07.004.

[27] J.W. Rhim, Kinetics of thermal degradation of anthocyanin pigment solutions driven from red flower cabbage, Food Sci. Biotechnol. 11 (2002) 361–364 (accessed December 1, 2022), https://www.dbpia.co.kr/journal/articleDetail?nodeId=NODE01794003.

[28] T. Yuan, T. Meng, P. He, Y. Shi, Y. Li, X. Li, L. Fan, S. Yang, Carbon quantum dots: an emerging material for optoelectronic applications, J. Mater. Chem. C Mater. 7 (2019) 6820–6835, https://doi.org/10.1039/C9TC01730E.

[29] Y. Zhao, X. Liu, Y. Yang, L. Kang, Z. Yang, W. Liu, L. Chen, Carbon dots: from intense absorption in visible range to excitation-independent and excitation-dependent photoluminescence, Fullerenes Nanotubes Carbon Nanostruct. 23 (2015) 922–929, https://doi.org/10.1080/1536383X.2015.1018413.

[30] S.J. Malode, M.M. Shanbhag, R. Kumari, D.S. Dkhar, P. Chandra, N.P. Shetti, Biomass-derived carbon nanomaterials for sensor applications, J. Pharm. Biomed. Anal. 222 (2023), 115102, https://doi.org/10.1016/j.jpba.2022.115102.

[31] V. Ţucureanu, A. Matei, A.M. Avram, FTIR spectroscopy for carbon family study, Crit. Rev. Anal. Chem. 46 (2016) 502–520, https://doi.org/10.1080/10408347.2016.1157013.
[32] H. Ding, S.-B. Yu, J.-S. Wei, H.-M. Xiong, Full-color light-emitting carbon dots with a surface-state-controlled luminescence mechanism, ACS Nano 10 (2016) 484–491, https://doi.org/10.1021/acsnano.5b05406.
[33] J. Liang, W. Li, J. Chen, X. Huang, Y. Liu, X. Zhang, W. Shu, B. Lei, H. Zhang, Antibacterial activity and synergetic mechanism of carbon dots against Gram-positive and negative bacteria, ACS Appl. Bio Mater. 4 (2021) 6937–6945, https://doi.org/10.1021/acsabm.1c00618.
[34] F. Cui, Y. Ye, J. Ping, X. Sun, Carbon dots: current advances in pathogenic bacteria monitoring and prospect applications, Biosens. Bioelectron. 156 (2020), 112085, https://doi.org/10.1016/j.bios.2020.112085.
[35] M. Varghese, M. Balachandran, Antibacterial efficiency of carbon dots against Gram-positive and Gram-negative bacteria: a review, J. Environ. Chem. Eng. 9 (2021), 106821, https://doi.org/10.1016/j.jece.2021.106821.
[36] M. Saif, H.F. El-Shafiy, M.M. Mashaly, M.F. Eid, A.I. Nabeel, R. Fouad, Synthesis, characterization, and antioxidant/cytotoxic activity of new chromone Schiff base nano-complexes of Zn(II), Cu(II), Ni(II) and Co(II), J. Mol. Struct. 1118 (2016) 75–82, https://doi.org/10.1016/j.molstruc.2016.03.060.
[37] A.A. Oun, J.W. Rhim, Preparation and characterization of sodium carboxymethyl cellulose/cotton linter cellulose nanofibril composite films, Carbohydr. Polym. 127 (2015) 101–109, https://doi.org/10.1016/j.carbpol.2015.03.073.
[38] S. Huang, B. Liu, D. Ge, J. Dai, Effect of combined treatment with supercritical CO2 and rosemary on microbiological and physicochemical properties of ground pork stored at 4 °C, Meat Sci. 125 (2017) 114–120, https://doi.org/10.1016/j.meatsci.2016.11.022.
[39] V. Kumar, M.K. Chatli, R.V. Wagh, N. Mehta, P. Kumar, Effect of the combination of natural antioxidants and packaging methods on quality of pork patties during storage, J. Food Sci. Technol. 52 (2015) 6230–6241, https://doi.org/10.1007/s13197-015-1734-2.
[40] N.S. Jagtap, R.V. Wagh, M.K. Chatli, O.P. Malav, P. Kumar, N. Mehta, Chevon meat storage stability infused with response surface methodology optimized Origanum vulgare leaf extracts, Agric. Res. 9 (2020) 663–674, https://doi.org/10.1007/s40003-020-00464-5.
[41] P.S. Nassos, A.D. King, A.E. Stafford, Relationship between lactic acid concentration and bacterial spoilage in ground beef, Appl. Environ. Microbiol. 46 (1983) 894–900, https://doi.org/10.1128/aem.46.4.894-900.1983.
[42] J.M. Jay, K.S. Kontou, Evaluation of the extract-release volume phenomenon as a rapid test for detecting spoilage in beef, Appl. Microbiol. 12 (1964) 378–383, https://doi.org/10.1128/am.12.4.378-383.1964.
[43] S. Akhavan Mahdavi, S.M. Jafari, E. Assadpoor, D. Dehnad, Microencapsulation optimization of natural anthocyanins with maltodextrin, gum arabic and gelatin, Int. J. Biol. Macromol. 85 (2016) 379–385, https://doi.org/10.1016/j.ijbiomac.2016.01.011.